

# Spectroscopy of GRB 021004: a structured jet ploughing through a massive stellar wind

R. L. C. Starling<sup>1</sup>, R. A. M. J. Wijers<sup>1</sup>, M. A. Hughes<sup>2</sup>, N. R. Tanvir<sup>2</sup>,  
P. M. Vreeswijk<sup>3</sup>, E. Rol<sup>4</sup> & I. Salamanca<sup>1</sup>

<sup>1</sup>*Astronomical Institute ‘Anton Pannekoek’, University of Amsterdam, Kruislaan 403, 1098 SJ Amsterdam, The Netherlands*

<sup>2</sup>*Centre for Astrophysics Research, STRI, University of Hertfordshire, College Lane, Hatfield, Herts. AL10 9AB, UK*

<sup>3</sup>*European Southern Observatory, Alonso de Córdova 3107, Casilla 19001, Santiago 19, Chile*

<sup>4</sup>*Dept. of Physics and Astronomy, University of Leicester, University Road, Leicester LE1 7RH, UK*

Accepted . Received ; in original form 2005 January 06

## ABSTRACT

We present spectra of the afterglow of GRB 021004 taken with WHT ISIS and VLT FORS1 at three epochs spanning 0.49–6.62 days after the burst. We observe strong absorption likely coming from the host galaxy, alongside absorption in H I, Si IV and C IV with blueshifts of up to 2900 km s<sup>−1</sup> from the explosion centre which we assume originates close to the progenitor. We find no significant variability of these spectral features. We investigate the origin of the outflowing material and evaluate various possible progenitor models. The most plausible explanation is that these result in the fossil stellar wind of a highly evolved Wolf-Rayet star. However, ionization from the burst itself prevents the existence of H I, Si IV and C IV close to the afterglow surface where the fast stellar wind should dominate, and large amounts of blueshifted hydrogen are not expected in a Wolf-Rayet star wind. We propose that the Wolf-Rayet star wind is enriched by a hydrogen-rich companion, and that the GRB has a structured jet geometry in which the gamma rays emerge in a small opening angle within the wider opening angle of the cone of the afterglow. This scenario is able to explain both the spectral line features and the irregular light curve of this afterglow.

**Key words:** gamma rays: bursts – techniques: spectroscopic – stars: winds, outflows

## 1 INTRODUCTION

The location of Gamma-ray bursts (GRBs) at cosmological distances was settled by the measurement of absorption lines in optical afterglow spectra, first done for GRB 970508 (Metzger et al. 1997). Many bursts are now followed up spectroscopically, not only for redshift determination but also as a probe of conditions in the host galaxy, the circumburst environment and intervening material. Spectral features imprinted on the afterglow spectrum can be a useful tool for understanding Gamma-ray Burst origins. In several, and at least 2, cases afterglow spectroscopy, sometimes in combination with photometry, has revealed the presence of a supernova connected with the GRB (e.g. GRB 980425 and SN1998bw, Galama et al. 1998; GRB 011121 and SN2001ke, Garnavich et al. 2003; GRB 030329 and SN2003dh, Hjorth et al. 2003; Stanek et al. 2003 and GRB 031203 and SN2003lw, Malesani et al. 2004).

GRB 021004 was detected on 2002 October 4, 12:06 UT by the HETE-2 satellite (Shirasaki et al. 2002). An optical afterglow was discovered ten minutes after detection of the prompt gamma-ray emission with an *R* band magnitude of

15.34 (Fox et al. 2002a). Intervening absorption systems at  $z = 1.38$  and  $z = 1.60$  were found in the subsequent afterglow spectra (Fox et al. 2002b), and later spectra showed further absorption features at redshift  $z = 2.323$  taken to be the host galaxy redshift (Chornock & Filippenko 2002). The afterglow light curve is not simply a power law in shape, but shows several bumps, particularly in the well sampled region around 1 day after the burst (Fig. 1). The temporal decay at early times (before  $\sim 1$  day) follows what is expected for a jet expanding into a stellar wind medium with a  $1/r^2$  dependence (Li & Chevalier 2003), but when including the later times several different explanations are possible.

GRB 021004 was localised in the optical band very early, allowing unusually prompt spectroscopic follow-up. The optical afterglow is bright, and rich in line features including Si IV and C IV. It is the first afterglow for which the spectrum is dominated by absorption lines spanning a 3000 km s<sup>−1</sup> velocity range, first reported by Salamanca et al. (2002). A number of high redshift afterglow spectra show absorption features from Si IV and C IV in their spectra, including GRB 000926 (Castro et al. 2003), GRB 011211

arXiv:astro-ph/0501120v2 23 Mar 2005

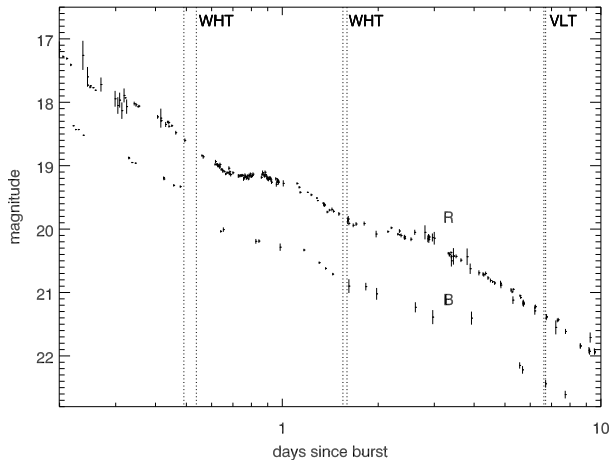


**Figure 1.** *B* and *R* band photometry of GRB 021004 compiled from the literature (Bersier et al. 2003, Fox et al. 2003, Holland et al. 2003, Pandey et al. 2003 and Uemura et al. 2003). The coverage of the WHT and VLT spectra presented here is shown by vertical dotted lines.

(Holland et al. 2002) and GRB 030323 (including an outflowing system with  $v = 130 \pm 60 \text{ km s}^{-1}$ , Vreeswijk et al. 2004). Such lines are also common in the interstellar medium (ISM) of many galaxies and also in a composite spectrum of  $z \sim 3$  Lyman Break galaxies (Shapley et al. 2003), but in these cases never reach the high velocities observed in the afterglow of GRB 021004. Despite many detailed studies of afterglow spectra of GRB 021004, the origin of the spectral features remains unclear.

We present early afterglow spectra taken with the 4.2-m William Herschel Telescope (WHT) and late-time spectra taken with the 8.2-m Very Large Telescope (VLT). Spectra were obtained 11.78 hours after the burst - the earliest optical spectra of GRB 021004 taken by a 4-m class telescope, and also at 1.55 and 6.62 days after the burst. We analyse in detail the multiple absorption complexes at all three epochs, and investigate their origins.

## 2 OBSERVATIONS

The WHT spectra were taken on 2002 October 4, 23:52:60 UT and October 6, 01:23:55 UT with the ISIS spectrograph. Overlapping blue (B300B) and red (R316R+GG495 filter) gratings were used with the EEV12 and Marconi2 CCDs respectively. Two exposures totalling 4000 s at epoch 1 and 4800 s at epoch 2 were taken with each grating, and with slits of width 0.87 arcsec at epoch 1 and 1.03 arcsec at epoch 2.

Flat fields were taken during the first night, and CuNe+CuAr arc lamps were obtained before and after each set of target exposures. The standard stars SP0305+261 and SP2323+157 were observed directly preceding or following each set of target and arc exposures on both nights. The airmass ranged between 1.01 and 1.09 and conditions were not photometric. We applied a correction for atmospheric extinction using the mean extinction curve for La Palma, and a Galactic extinction correction using  $E(B - V) = 0.060$  as determined by Schlegel, Finkbeiner & Davis (1998). Data

reduction was performed using IRAF, except for cosmic ray removal, where we used the L. A. Cosmic routine to remove both point source and irregular-shaped cosmic ray traces (van Dokkum 2001). For each night, we combine the individual exposures of GRB 021004 to achieve a higher signal to noise.

The useful remaining wavelength ranges are 3650–6000 Å for the blue grating and 6500–8500 Å for the red grating. The wavelength resolution is approximately 2.2 Å at epoch 1 and 3.5 Å at epoch 2. The average signal to noise is 12.7 at epoch 1, 7.6 at epoch 2.

A third epoch observation was made with the Very Large Telescope (VLT-Antu) in Paranal on 2002 October 11, 02:57:09 UT. The observations were made with the Focal Reducer/Low Dispersion Spectrograph 1 (FORIS1) instrument in the Longslit Spectroscopy (LSS) mode. Six 1200 s exposures were taken through a  $0.7 \times 416.8$  arcsec slit, with the 600B grism (3450–5900 Å). Data reduction was carried out using a combination of routines within the IRAF and Starlink FIGARO packages. The 6 object images were combined into a single spectrum. Wavelength calibration was performed using He and HgCd lamps, and the standard star LTT 7987 was used for flux calibration with airmasses ranging from 1.38–1.57. The resulting spectrum has a signal to noise ratio of 4.6 at the longest wavelengths down to  $\sim 2.5$  at H Ly $\alpha$ , and a wavelength resolution of  $\sim 3.8$  Å.

Spectral analysis was done using the Starlink DIPSO spectral fitting package. To obtain the correct continuum fluxes, the data are compared with *B* and *R* band photometry collected from the literature (Fig. 1). The photometric points closest to the observation dates were interpolated to give the magnitudes  $B_{\text{epoch1}} \sim 19.50$ ,  $B_{\text{epoch2}} \sim 20.83$  and  $R_{\text{epoch1}} \sim 18.55$  expected in the WHT spectra and  $B \sim 22.44$  at the time of the spectroscopic VLT observation. The observed fluxes in the WHT spectra are as expected at epoch 2, but the earlier spectra are fainter by a factor 2.2 for the blue grating and 1.7 for the red grating. The flux in the VLT spectrum is 1.6 times lower than expected from photometric measurements.

### 2.1 Spectral line fitting

We show the first epoch WHT ISIS spectrum and its error spectrum in Fig. 2 with all identified lines labelled. We fit a local continuum around each line complex with a first order polynomial. Each doublet was modelled with two Gaussian profiles, with the line full widths at half maxima (FWHM) of the two components tied. For each species, all doublet fits (fit parameters of FWHM, central wavelength and peak intensity) were optimised simultaneously using the least squares method. The H Ly $\alpha$  region has to be treated differently as individual lines are much less clear, so here we fitted a number of broad absorption troughs representing some unknown number of blended lines, plus the narrow emission line. The error on line equivalent widths was measured within the DIPSO package using the statistical uncertainties in the continuum fit and on the flux values within the line, and also the systematic error in continuum placement and zero level in the case of the WHT data (Howarth & Phillips 1986).

**Table 1.** Model fits to the identified spectral line complexes at both epochs. Velocities and equivalent widths are in the restframe of the source. EW errors are quoted at the  $2\sigma$  level and EWs marked with a \* indicate lower limits for saturated lines. + indicates the two heavily blended lines of CIV for which only the total EW should be considered. Velocities and redshifts are given to  $1\sigma$  accuracy and precision of observed wavelengths is limited by the wavelength resolutions specified in Section 2. Epochs 1 and 2 refer to WHT ISIS data, epoch 3 refers to VLT FORS1 data.

$\lambda_{\text{obs}}$ (Å)	Line	epoch	$z$	$v_{\text{internal}}$	FWHM (km s $^{-1}$ )	EW (Å)	$v_{\text{outflow}}$ (km s $^{-1}$ )	system
3959,3969,3976,3982	see text for ID	1		<350>		2.44±0.32		
3959,3969,3976,3982		2		<330>		2.11±0.70		
4006	Ly $\alpha$ $\lambda$ 1215 Å	1	2.297±0.002	410±45		1.52±0.27*	2700±170	IV
4005		2	2.296±0.003	450±250		1.28±0.62*	2800±270	
4008		3	2.297±0.003	360±40		2.37±0.87*	2700±290	
4013	Ly $\alpha$ $\lambda$ 1215 Å	1	2.303±0.002	670±140		1.96±0.35	2200±170	III
4011		2	2.301±0.003	620±450		2.25±1.02	2400±270	
4028	C IV $\lambda$ 1548 Å	1	1.602±0.001	240±70		0.60±0.16	intervening	
4026		2	1.601±0.002	230±60		0.71±0.42	intervening	
4028		3	1.602±0.003	240±40		1.54±0.99	intervening	
4037	Ly $\alpha$ $\lambda$ 1215 Å	1	2.323±0.001	740±160		2.83±0.48	360±170	II
4036		2	2.322±0.003	690±100		2.48±1.12	450±270	
4037		3	2.321±0.003	400 fixed		2.09±1.01	560±280	
4045	Ly $\alpha$ $\lambda$ 1215 Å	1	2.329±0.002	350±80		1.39±0.25*	-180±170	I
4044		2	2.328±0.003	280±70		0.97±0.49*	-90±270	
4043		3	2.326±0.003	220±40		0.65±0.70*	50±280	
4346	Al II $\lambda$ 1670 Å	1	1.602±0.001	350±80		0.68±0.15	intervening	
4346		2	1.602±0.002	280±70		0.57±0.31	intervening	
4596	Si IV $\lambda$ 1393 Å	1	2.297±0.002	230±70		0.23±0.09	2700±150	IV
4596		2	2.297±0.003	110±40		0.13±0.13	2700±230	
4598		3	2.298±0.003	60±20		0.28±0.39	2600±250	
4622	Si IV $\lambda$ 1402 Å	1	2.296±0.002	230±70		0.26±0.10	2800±150	
4624		2	2.295±0.003	110±40		0.14±0.12	2900±230	
4623		3	2.296±0.003	150±30		0.51±0.42	2800±250	
4628	Si IV $\lambda$ 1393 Å	1	2.320±0.002	220±20		0.57±0.12	630±150	II
4628		2	2.320±0.003	350±50		0.96±0.40	630±230	
4629		3	2.321±0.003	290±60		0.56±0.48	520±250	
4658	Si IV $\lambda$ 1402 Å	1	2.320±0.002	220±20		0.33±0.10	630±150	
4658		2	2.320±0.003	340±50		0.41±0.22	630±230	
4660		3	2.322±0.003	290±60		0.26±0.52	430±240	
4637	Si IV $\lambda$ 1393 Å	1	2.327±0.002	300±10		1.13±0.20	0±150	I
4637		2	2.326±0.003	270±20		1.05±0.42	90±230	
4637		3	2.327±0.003	250±20		1.38±0.51	-20±250	
4667	Si IV $\lambda$ 1402 Å	1	2.327±0.002	300±10		1.04±0.19	0±150	
4667		2	2.326±0.003	260±20		1.03±0.41	90±230	
4668		3	2.327±0.003	250±20		1.11±0.51	-40±240	
5102	C IV $\lambda$ 1548 Å	1	2.296±0.001	230±20		0.60±0.11	2800±130	IV
5102		2	2.296±0.002	310±60		0.60±0.26	2800±210	
5102		3	2.295±0.003	270±30		0.71±0.12	2900±230	
5106	C IV $\lambda$ 1550 Å	1	2.296±0.001	230±20		0.39±0.08	2800±130	
5106		2	2.296±0.002	310±60		0.51±0.23	2800±210	
5108		3	2.294±0.003	270±30		0.30±0.11	3000±230	
5111	C IV $\lambda$ 1548 Å	1	2.302±0.001	190±20		0.38±0.08	2300±130	III
5111		2	2.302±0.002	120±20		0.20±0.12	2300±210	
5113		3	2.302±0.003	100±20		0.27±0.09	2300±220	
5114	C IV $\lambda$ 1550 Å	1	2.300±0.001	190±20		0.23±0.07	2500±130	
5114		2	2.300±0.002	120±20		0.21±0.12	2500±210	
5117		3	2.300±0.003	100±20		0.23±0.09	2500±220	
5141	C IV $\lambda$ 1548 Å	1	2.321±0.001	340±10		1.79±0.28*	540±130	II
5140		2	2.320±0.002	330±100		1.53±0.57*	630±210	
5141		3	2.321±0.003	220±20		1.68±0.13*	670±220	
5149	C IV $\lambda$ 1550 Å <sup>+</sup>	1	2.321±0.001	330±10		1.06±0.17*	540±130	
5148		2	2.319±0.002	330±100		0.64±0.27*	720±210	
5150		3	2.321±0.003	300±10		1.90±0.12*	900±220	
5152	C IV $\lambda$ 1548 Å <sup>+</sup>	1	2.328±0.001	310±10		1.28±0.21*	-90±130	I
5150		2	2.327±0.002	340±30		2.09±0.77*	0±210	
5156		3	2.330±0.003	300±10		0.48±0.11*	50±220	
5160	C IV $\lambda$ 1550 Å	1	2.329±0.001	310±10		1.64±0.26*	-180±130	
5159		2	2.329±0.002	340±30		1.89±0.70*	-180±210	
5160		3	2.328±0.003	300±10		1.31±0.11*	-20±220	
5559	Al II $\lambda$ 1670 Å	1	2.327±0.001	160±10		0.59±0.13	0±120	I
5559		2	2.327 fixed	100±30		0.19±0.16	0±190	
5576,5650,5669	Fe II $\lambda$ 2344,2374,2382 Å	1	1.380±0.001	<160±20>		2.25±0.33	intervening	
5576,5650,5669		2	1.380±0.001	<100±30>		2.34±0.73	intervening	
6654	Mg II $\lambda$ 2796 Å	1	1.380±0.001	230±10		1.52±0.26	intervening	
6671	Mg II $\lambda$ 2803 Å	1	1.380±0.001	250±20		1.23±0.22	intervening	
6731	Fe II $\lambda$ 2586 Å	1	1.603±0.001	130±30		0.34±0.10	intervening	
6765	Fe II $\lambda$ 2599 Å	1	1.603±0.001	220±20		0.74±0.16	intervening	
7278	Mg II $\lambda$ 2796 Å	1	1.603±0.001	220±70		1.27±0.23	intervening	
7296	Mg II $\lambda$ 2803 Å	1	1.603±0.001	210±40		1.54±0.27	intervening	

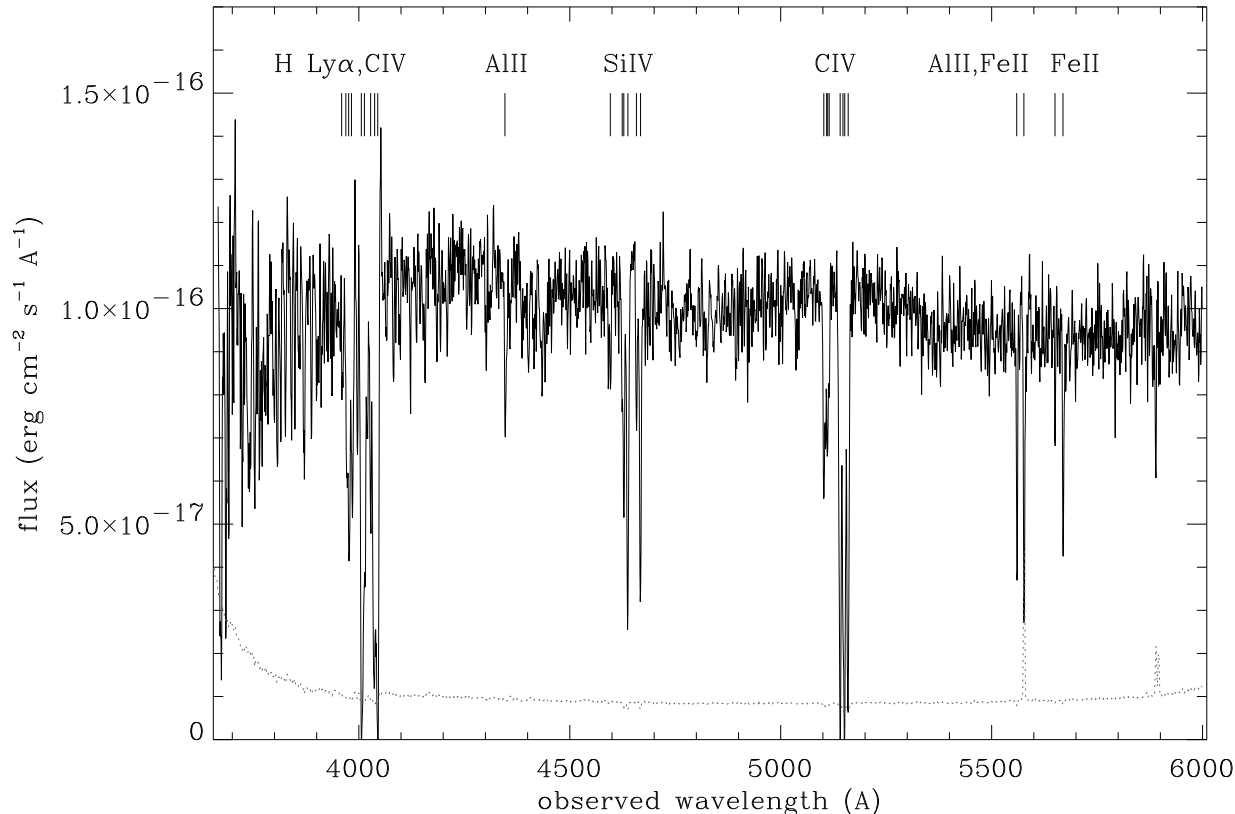


**Figure 2.** The WHT blue grating spectrum at epoch 1 (solid line) and the error spectrum (dashed line), fluxes corrected according to photometric light curve in Fig. 1. Identified lines are labelled above.

### 3 RESULTS

The results of spectral fitting are detailed in Table 1. We observe H Ly $\alpha$ , Si IV and CIV absorption features at 3 redshifts, and H Ly $\alpha$  and CIV at a further redshift (this is the weakest velocity system and is not detected in Si IV or Ly $\alpha$  at epoch 3), all around  $z \sim 2.3$ . Other than the intervening systems, all absorption lines have a component at  $z = 2.327$ , the highest redshift absorption system we observe, which we take to be the redshift of the host galaxy. If the other 3 systems are a type of outflow (we do not rule out the possibility that the 0 velocity system is associated with the GRB progenitor rather than the host galaxy, but see Section 4.2), their observed velocities would be approximately 570, 2400 and 2800 km s $^{-1}$  (as reported in Salamanca et al. 2002).

The lines at we observe at 1190–1197Å could be either H Ly $\alpha$  at 5500 km s $^{-1}$ , intervening Ly $\alpha$  forest lines or Si II at 0 km s $^{-1}$  ( $z = 2.327 \pm 0.003$ ). In the former case, we might expect to see CIV or Si IV at this velocity as well, which we do not; in the latter case, the stronger Si II  $\lambda$ 1260 line should also be seen, but it is not. We conclude that the nature of the lines at 1190–1197Å is uncertain, though most likely Ly $\alpha$  forest lines, so we claim no H at velocities above 3000 km s $^{-1}$ .

#### 3.1 Variability

We find no significant variability in equivalent width (EW, within the  $2\sigma$  errors) between the absorption features com-

mon to 2 or more epochs, with the exception of Al II  $\lambda$ 1670 at  $z = 2.327$  which we were unable to clearly detect in the 2nd and 3rd epochs. Fixing the position of Al II to that found at epoch 1 allowed us to fit a line there, and the resulting EW is inconsistent with that at epoch 1 within the  $2\sigma$  errors. The Al II line is also detected in several other spectra of this afterglow (Møller et al. 2002; Matheson et al. 2003; Mirabal et al. 2003; Schaefer et al. 2003; Fiore et al. 2004) taken at times both before (in the case of the 2.56-m Nordic Optical Telescope (NOT) data) and after our 2nd epoch WHT spectra, and in each case the measured EW is consistent with what we measure in the epoch 1 WHT data. The discrepancy may be due to imperfect cosmic ray/bad column removal at epoch 2, and/or there may be moderate variability in this line. Fe II  $\lambda$ 2344 is another low ionization line which is not detected in all optical spectra of GRB 021004, though we do find it in the first 2 epochs presented here. The apparent variability of this line is largely due to the presence of a strong skyline near that position. The lack of significant variability in the strong lines indicates that the absorbing material in our line-of-sight remains in front of the afterglow throughout the  $\sim 6$  days spanned by our spectra.

The EWs we measure are consistent with those of corresponding lines or line complexes reported by Møller et al. (2002), Matheson et al. (2003), Mirabal et al. (2003) and Fiore et al. (2004). The resolution of these spectra are such that we are not resolving every component of each line blend – the line complex at the host galaxy redshift is resolved

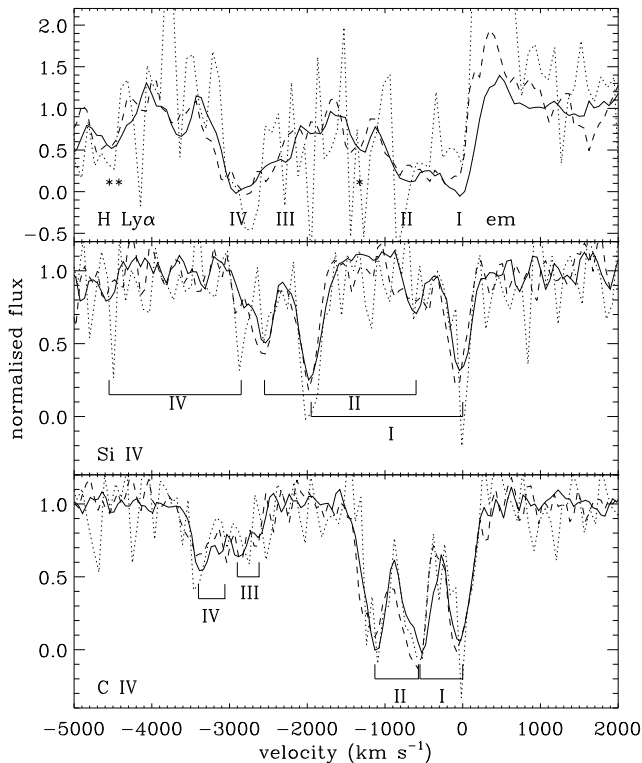


**Figure 3.** Outflow velocities of the C IV and Si IV absorption doublets (velocities plotted are for the longer wavelength components only) and corresponding hydrogen Ly $\alpha$  systems, divided by the local continua. The solid lines show the WHT observation of 4/10/02, the dashed lines show the WHT observation of 6/10/02 and the dotted lines show the VLT observation of 11/10/02. The 4 velocity systems are denoted by roman numerals, the Ly $\alpha$  emission line (too large in the VLT data to be shown fully on this plot) is labelled ‘em’. Intervening C IV is marked with a \* and \*\* marks the long-wavelength end of the bluest absorption complex.

into 3 components in the VLT UVES spectrum (Fiore et al. 2004). Unfortunately the calibration uncertainties in our late-time spectrum are too large to detect the colour change blueward of Ly $\alpha$  of  $\sim 0.3$  magnitudes claimed by Matheson et al. (2003) and Schaefer et al. (2003) and supported by photometric observations (Bersier et al. 2003), but not found in the HST observations of Fynbo et al. (2004).

### 3.2 Hydrogen Ly $\alpha$ emission

We clearly detect the host galaxy ISM through its emission in hydrogen Ly $\alpha$ . Taking the host galaxy redshift to be  $z = 2.327$ , the Ly $\alpha$  emission line centre then appears redshifted, by an amount that is somewhat different between various authors. However, as it lies right on the edge of the Ly $\alpha$  absorption complex, which probably eats into the emission line, its central wavelength will depend on the resolution of the spectrum, so this effect is not surprising. Within the resolution of these spectra (a few hundred  $\text{km s}^{-1}$ ), its velocity is in fact consistent with zero.

The Ly $\alpha$  emission line strength is difficult to estimate due to the line blending. However, by fitting in isolation the part of the line observed above the continuum level, we can

measure a lower limit to the flux:

$F_{\text{epoch 1}} \geq 2.35 \pm 0.87 \times 10^{-16} \text{ erg cm}^{-2} \text{ s}^{-1}$ ,  $F_{\text{epoch 2}} \geq 1.66 \pm 0.34 \times 10^{-16} \text{ erg cm}^{-2} \text{ s}^{-1}$ . These lower limits are consistent within the quoted  $1\sigma$  errors, suggesting that both the emission line and the blended absorption line component at the host redshift show no variability, and are consistent with the value measured in NOT data of this source (Møller et al. 2002). In epoch 3 we obtain  $F_{\text{epoch 3}} \geq 1.17 \times 10^{-16} \text{ erg cm}^{-2} \text{ s}^{-1}$ , with a large error of  $\sim 56$  per cent.

Following the method described in Fynbo et al. (2004, and references therein) we calculate a star formation rate (SFR) using the Ly $\alpha$  emission line flux measured in the WHT data. We find a lower limit for the SFR of  $6 M_{\odot} \text{ yr}^{-1}$ , with average values of 10 and  $7 M_{\odot} \text{ yr}^{-1}$  at epochs 1 and 2 respectively, consistent with estimates based on Keck and HST data of this afterglow (Djorgovski et al. 2002; Fynbo et al. 2004). Our estimate assumes a cosmology with  $H_0 = 70 \text{ km s}^{-1} \text{ Mpc}^{-1}$ ,  $\Omega_M = 0.3$  and  $\Omega_{\Lambda} = 0.7$ .

From these data we can obtain only a lower limit for the column density of H I of  $N_{\text{HI}} \geq 10^{14} \text{ cm}^{-2}$ , by comparing the observed EWs of each line to their theoretical curves of growth. This poor constraint is because the H I lines are close to or at saturation, they are all heavily blended and cannot be well modelled. The column of neutral hydrogen is in fact much larger:  $1 \times 10^{18} \leq N_{\text{HI}} (\text{cm}^{-2}) \leq 1.1 \times 10^{20}$  (Møller et al. 2002; Fynbo et al. 2004). From the unsaturated lines of Si IV and C IV (those at the 2 lowest redshifts and part of the outflow) we measure columns of  $\log N = 14.0 \pm 0.9$  and  $14.6 \pm 0.9$  respectively, where  $N$  is given in  $\text{cm}^{-2}$ , in line with previous estimates (Schaefer et al. 2003 C IV only; Fiore et al. 2004).

## 4 DISCUSSION

The spectra we have taken provide information on material whose distance from the explosion centre covers a wide range. No material can be closer than the emitting surface (the blast wave) at the time of the first spectrum, which is about  $10^{16} \text{ cm}$ . Some lines are from intervening galaxies very far from the host at  $z = 1.38$  and  $1.60$ , and yet others are from the host itself at  $z = 2.327$ . We interpret the low-ionization absorption lines and the narrow Ly $\alpha$  emission line around  $z \simeq 2.33$  as coming from within the host, but many parsecs from the explosion so that the absorbing material was unaffected by the explosion or by the GRB progenitor. The blueshifted lines we interpret as coming from the region affected by the explosion or the progenitor, which we shall term the ‘high-velocity zone’. The Ly $\alpha$  absorption could in principle come from either the high-velocity zone or the host, but given its velocity structure, identical to that of the high-ionization lines of Si IV and C IV, we shall interpret it as coming from the high-velocity zone. Ly $\beta$  absorption has also been observed with components spanning approximately the same velocity range (Mirabal et al. 2003). Note that this implies a very low column of H I in the host in front of the immediate star forming region of the GRB progenitor, unlike other GRB hosts observed to-date. We discuss these outflowing systems and their possible origins in turn below.

#### 4.1 Intervening systems, overdense regions and partial covering

There is a possibility that the ‘outflow’ may just be several systems in the line of sight to the burst. This, however, seems highly unlikely to occur so close to the burst redshift (see Schaefer et al. 2003; Fiore et al. 2004) and in addition to the  $z = 1.38$  and  $1.60$  systems. Specifically, a number of (proto-)galaxies within  $3000 \text{ km s}^{-1}$  of each other would constitute a nonlinearly collapsed overdensity that is very hard to get as early as  $z \simeq 2.3$  in currently favoured cosmologies either in the Hubble flow or within a galaxy cluster including the GRB host.

Let us now consider a clumpy stellar wind environment for GRB 021004. Clumps of material may comprise the stellar wind – Cherepashchuk (1990) suggested that up to 80 per cent of a Wolf-Rayet stars’ mass can be lost in clumps in the wind. In principle the lines we see could either be due to a wind with optical depth less than 1 absorbing a fraction of the light more or less uniformly throughout the wind material, or by a partial covering of the emitting surface by optically thick clouds. In the latter case, the spectrum should be the sum of a featureless continuum from regions uncovered by cloud, and a spectrum with saturated, flat-bottomed lines from the regions covered by clouds that are optically thick in the lines but thin in the continuum. This implies that the summed spectrum should have flat-bottomed lines whose flux level in the centre is non-zero, when viewed with high enough resolution spectroscopy. Whilst our data do not allow us to address this distinction, the UVES high resolution afterglow spectra of GRB 021004 (Fiore et al. 2004; Castro-Tirado et al., in preparation) show flat-bottomed, saturated lines with no flux in the centre, effectively ruling out a partial covering model.

We now consider the exotic possibility that the high-velocity absorption features are from a number of supernova shells produced by an earlier stellar death in the same cluster that produced the progenitor of the GRB. It is plausible that an unusually rich cluster (e.g. the central cluster of the S Dor complex in the Large Magellanic Cloud, LMC) would have produced a number of stellar explosions in the past Myr, of which the supernova remnants are now expanded beyond the cluster core size, so that our line of sight to the next explosion will only pass through the approaching sides of the shells and thus give rise to blueshifted features. The hydrogen richness is explained in this case, since the ejecta could contain hydrogen, or sweep it up. The problem is that the velocities are low enough that supernova shells must have significantly decelerated. In so doing, they will shock and be heated to X-ray temperatures, which makes species like H I, Si IV and C IV rather unlikely to be present in those shells. The shell geometry has also been seen around Wolf-Rayet stars as shell nebulae. Mirabal et al. (2003) demonstrated that optical absorption lines like those seen in GRB 021004 can be produced by a fragmented shell nebula, under very particular conditions. The shell nebula would need to have been located at a distance from the GRB progenitor such that it received sufficient radiative acceleration from the burst to achieve the high velocities, but was not fully ionized by the GRB flux. All things considered, we do not favour these options.

#### 4.2 A single star as progenitor

The most natural explanation for the blueshifted absorption features is that they arise in a stellar wind. A  $1/r^2$  density profile is inferred from the light curve at very early times (Li & Chevalier 2003) suggesting a stellar wind circumburst medium. A GRB progenitor must be a massive, evolved star. The highest velocity system observed is an outflow of  $\sim 2800 \text{ km s}^{-1}$ , which could be the terminal velocity of a stellar wind and in this case implies the star is a Wolf-Rayet (WR) star (Mirabal et al. 2003; Schaefer et al. 2003). Such stars evolve to type Ib supernovae and are characterised by large mass loss rates in high velocity, optically thick stellar winds. The 3 outflow velocities observed in this afterglow could correspond to the fast WR wind ( $2800 \text{ km s}^{-1}$ ), a slower wind from an earlier phase in the stellar lifetime ( $2400 \text{ km s}^{-1}$ ) and the slow bubble moving into the ISM or mixing of winds from different phases ( $570 \text{ km s}^{-1}$ ) as shown in simulations of massive star evolution by Van Marle, Langer & García-Segura (2005). Massive star winds are predicted to show a higher optical depth in the CIV line than in the Si IV line (Leitherer & Lamers 1991) which seems to be true for these data. Line-locking is a characteristic of WR wind spectra, since the winds are radiatively driven (e.g. Puls et al. 1996), and this appears to be present in the WHT spectra (Møller et al. 2002), seen as an overlap of the CIV doublet lines at the two highest redshifts. If, however, the only signature of the radiatively driven WR wind is the fastest absorption component, then line-locking would not be expected, and would be a coincidence in this case.

There are two basic challenges to interpreting these lines as originating in the stellar wind. The first is that the species causing the lines must survive the initial blast of UV to gamma rays without becoming fully ionized. The distance out to which the material might be fully ionized can be estimated in two different ways, depending on the recombination time-scale. If the recombination time is short compared to the 100 s duration of the ionizing flash (Shirasaki et al. 2002), we can use ionization equilibrium as characterised by the ionization parameter  $\xi = L/nr^2$ .

If on the other hand the recombination time is long, then a given atom with cross-section  $\sigma$  for ionization will simply absorb at least one ionizing photon:

$$\sigma_i \frac{E_{\text{tot}}}{4\pi r^2 < E_i} \geq 1 \quad (1)$$

This is the appropriate limit to use since a rough calculation of the recombination time for hydrogen gives a time-scale of the order of  $10^5$  years. This gives minimal distances for the survival of Si IV, C IV and H I of  $5 \times 10^{18}$ ,  $2 \times 10^{19}$  and  $9 \times 10^{20}$  cm respectively (using photoionization cross-sections and threshold energies from Verner et al. 1996 and  $E_{\text{tot}} = E_{\text{iso}}$ ). If we assume that these 3 species are co-located (because they have the same velocity structure) then the minimum distance out to which we could find them if they were ionized by the burst flux is far beyond the few pc radius of a typical stellar wind bubble. This excludes a stellar wind origin for these absorption lines if they are intercepted by the GRB flux.

The second challenge is the presence of hydrogen in the spectra with approximately the same velocity structure as Si IV and C IV, strongly suggesting that significant amounts of hydrogen are present in the stellar wind, with a column

of neutral hydrogen  $\geq 10^{14}$  cm $^{-2}$ . This is not usual for a WR wind. A WR star will once have been hydrogen-rich, and so the outer wind can have hydrogen, but its velocity structure will not match that of the later, hydrogen-deficient wind.

WR stars in our own galaxy are hydrogen deficient and in most cases H is not detected at all. However in the SMC a large fraction, if not all single WN-type WR stars (nitrogen-rich WR stars) show hydrogen in their spectra (Foellmi, Moffat & Guerrero 2003a). This was unexpected given the lack of H in Galactic WN-types, leading to the suggestion that the WN population in the SMC is fundamentally different from that of our own galaxy. So in the SMC, where the metallicity is low causing less severe mass loss and fewer WC-type (carbon-rich) WR stars, massive stars can remain H-rich in the WR phase. GRB host galaxies are thought to be metal-poor like the SMC, but the strength of C IV and Si IV and non-detection of nitrogen (particularly N IV, NV) in the afterglow spectra of GRB 021004 is inconsistent with a WN-type WR star. In fact carbon produces the strongest absorption features, suggesting we are observing the wind of a WC-type WR star (e.g. Mirabal et al. 2003; Schaefer et al. 2003), thought to be the last evolutionary stage of the WR phase. On the other hand we do not detect C III  $\lambda$ 1247 which is strongly detected in samples of WC-types with e.g. FUSE (Willis et al. 2004) and IUE (Nussbaumer et al. 1982).

There is no significant variability in the absorption line EWs between our very early spectrum at 0.49 days after burst, and those beginning 1.55 and 6.62 days after burst (besides the Al II line discussed in Section 3.2). The three epochs appear to be in different ‘phases’ of the peculiar afterglow light curve (Fig. 1). The jumps in the light curve at 0.8–1 and 2.5–3 days cannot then be shells through which the afterglow light passes, because the same absorption is seen at all epochs. Unless the shells are located very far from the star so that the afterglow never overtakes them, which then makes it difficult to produce the fast velocities we observe. 21-cm measurements have shown HI shells around WR stars, e.g. WR 102 (Gosachinskij & Lozinskaya 2002), but these have expansion velocities of  $\sim 50$  km s $^{-1}$ . The Galactic WR star WR 3 may also have an unusually high H content if it is a single star rather than in binary with an O star, but again only rather low velocities of up to 400 km s $^{-1}$  are observed (Marchenko et al. 2004), never reaching the 2400–2900 km s $^{-1}$  velocities we observe.

### 4.3 A binary system progenitor

So, whilst a WR star is the obvious choice to explain the blue shifted, line-locked absorption complexes, this picture is difficult to reconcile with the large amount of neutral hydrogen observed, particularly at very high velocities. This conundrum leaves us with few options. Either distant carbon-rich WR stars are very different to those in our own galaxy and are able to retain a large fraction of their hydrogen, or the hydrogen originates elsewhere – perhaps in a companion star wind. There is the possibility that we are seeing a WR star in a close binary with a hydrogen-rich main-sequence star. Even for an O star companion, the momentum loss rate  $\dot{M}v_\infty$  of the WR star far exceeds that of the companion, and so the wind velocity structure at distances much greater than the binary separation will be dominated by the

WR star. However, a few to 10 per cent of the mass will come from the companion and so is hydrogen rich. When mixed into the WR wind it can cause the observed phenomenon of H Ly $\alpha$  emission accompanying otherwise typical WR lines. The *a priori* probability that a WR star is in a binary with an O star is still a debatable number. Foellmi et al. (2003a) give theoretical binary frequency lower limits for WR+O systems in the Magellanic Clouds of  $0.41 \pm 0.13$  (LMC) and  $0.98 \pm 0.32$  (SMC), assuming a mass loss - metallicity relation of  $\dot{M} \propto Z^{0.5}$  and excluding rotation effects. They find, however, significantly lower observed fractions of 30 and 40 per cent respectively (Foellmi et al. 2003a,b). Various measured values point towards the conclusion that the binary frequency of WR stars is identical to that of their progenitors and independent of the metallicity.

There is also the possibility that the WR star is in a binary with a less massive star that is providing the observed hydrogen. The probability of a WR star having a lower-mass companion (perhaps 1–3  $M_\odot$ ) is even less well known, since such low-mass, low-luminosity companions are hard to detect. The only evidence for the existence of such binaries is the population of soft X-ray transients in our Galaxy, which consist of a black hole orbited by a low-mass star in a very tight orbit. Their ancestors must have been WR stars with a low-mass main-sequence binary companion. It has been suggested that these systems produce a GRB when the black hole forms (Lee, Brown & Wijers 2002).

One necessary consequence of this H-admixing model is that probably only within some angle from the orbital plane of the binary will H be mixed into the outflowing wind. In the polar direction pure WR composition will dominate. This will constrain our viewing angle to the system to being not too far out of the orbital plane. For an O star, still having a relatively strong wind, this is not severe, but for a low-mass star with a very weak wind, the system would have to be viewed at or close to edge-on. This is unlikely if, as predicted by the collapsar model, the jets emerge from the polar axis of the progenitor star.

### 4.4 A structured jet model

The ionization problem remains however, and it seems that in order to observe fast-moving species such as Si IV and C IV and even H I, one must be observing a region undisturbed by the gamma ray jet. In order to achieve this we suggest a structured jet geometry, with one narrow jet ( $\lesssim 3^\circ$ ) and one slower, much wider jet of material which are both visible to us (Fig. 4). In fact, the afterglow has a surface area, and so there are several lines-of-sight along which the light will reach us. Gamma rays from the inner jet will ionize material in its path. But if the inner jet opening angle is small then there will also be a line-of-sight along which we see material unaffected by high energy radiation. We propose that there is a second wider cone of slower jet material surrounding the narrow gamma ray jet. This wide jet is also seen through the absorber, probably a fast stellar wind within 2 older more slowly moving wind phases, which produces the absorption lines we observe.

The power law decay of afterglow light curves can be very smooth, as in the cases of GRB 020813 (e.g. Laursen & Stanek 2003) and GRB 990510 (e.g. Stanek et al. 1999). But some show considerable deviations from this with many ir-

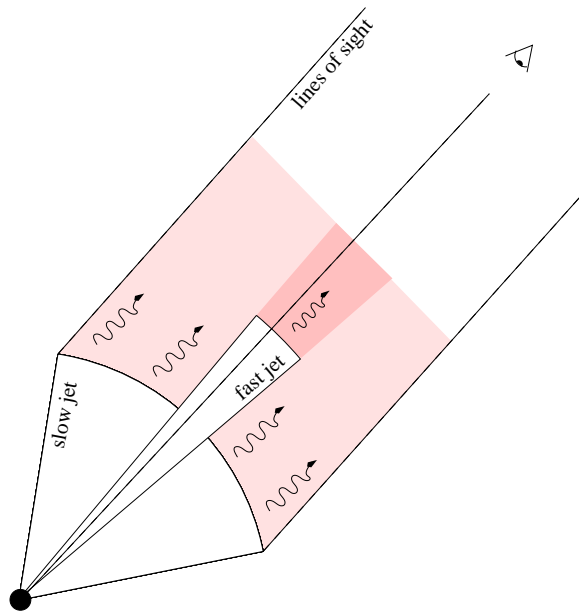


**Figure 4.** A sketch of the structured jet geometry within the stellar wind, where our lines-of-sight (dashed lines) intersect both fully ionized material in front of the narrow, fast jet (dark grey) and material ionized to a much lesser degree by the the slower jet (light grey).

regularities, as seen in GRB 011211 (e.g. Holland et al. 2002) and GRB 030329 (e.g. Lipkin et al. 2004) and this is the case for this burst (Fig 1). The structured jet scenario we describe is consistent with the observed light curve of the afterglow of GRB 021004 (Van der Horst, private communication). We also note that the general decay of the light curve may be adequately fit with other models including several energy injections (Björnsson, Gudmundsson & Johannesson 2004), patchy shell models (Nakar, Piran & Granot 2003) and density enhancements in the ISM (Lazzati et al. 2002) or in a wind (Heyl & Perna 2003).

From the light curve alone we cannot pinpoint the cause of the irregularities in the temporal decay. Considering the light curve in combination with the spectra provides further constraints and leads us to prefer the structured jet idea, which can explain both types of observation and does not require the absorbers to be at a large distance from the progenitor to produce the absorption lines seen in our spectra.

## 5 CONCLUSIONS

We have observed the optical afterglow of GRB 021004 spectroscopically at three epochs ranging from 0.49 to 6.62 days after the GRB, when the emitting surface is of order  $10^{16}$  cm away from the explosion centre. The most unique feature in the spectra is the fact that lines of HI, SiIV and CIV are observed at blueshifts of up to  $2900 \text{ km s}^{-1}$ . While no model explored by ourselves or earlier authors explains this phenomenon in a very simple manner, we find that by far the most plausible explanation is that these lines result in the fossil stellar wind of a highly evolved Wolf-Rayet star. It

is unusual that hydrogen would be present in such a wind. This could be explained if WR stars do remain hydrogen-rich up to explosion at high redshift and/or low metallicity, or if a nearby companion star had enriched the WR wind with hydrogen. In any case, our data seem to further enhance the case for the origin of GRBs in the core collapse of very massive stars. Ionization from the burst itself prevents the existence of HI, SiIV and CIV close to the afterglow surface where the fast stellar wind should dominate. A structured jet geometry is a promising explanation: the gamma rays emerge in a small opening angle leaving a wider cone of slower, less energetic material also along our line-of-sight. This wider jet does not fully ionize the material in its path, and can give rise to the absorption lines we observe. This model is able to explain both the spectral features and reproduce the light curve shape.

## 6 ACKNOWLEDGMENTS

We thank R. McLure for interrupting his observing run to take these WHT data. We acknowledge useful discussions with C. Dijkstra, M. Franx, A. J. van der Horst, A. de Koter, A.-J. van Marle and K. Wiersema. The WHT is operated on the island of La Palma by the Isaac Newton Group in the Spanish Observatorio del Roque de los Muchachos of the Instituto de Astrofísica de Canarias. The VLT data were obtained under ESO proposal number 70.D-0523(A). The authors acknowledge benefits from collaboration within the Research Training Network ‘Gamma-Ray Bursts: An Enigma and a Tool’, funded by the EU under contract HPRN-CT-2002-00294.

## REFERENCES

- Bersier D. et al., 2003, *ApJ*, 584, L43
- Björnsson G., Gudmundsson E. H., Johannesson G., 2004, *ApJ*, 615, L77
- Castro S., Galama T. J., Harrison F. A., Holtzmann J. A., Bloom J. S., Djorgovski S. G., Kulkarni S. R., 2003, *ApJ*, 586, 128
- Cherepashchuk A. M., 1990, *Astron. Zh. (USSR)*, 67, 955
- Chornock R., Filippenko A. V., 2002, GCNC 1605
- Djorgovski S. G. et al., 2002, GCNC 1620
- Fiore F. et al., 2004, *ApJ*, in press (astro-ph/0409717)
- Foellmi C., Moffat A. F. J., Guerrero M. A., 2003a, *MNRAS*, 338, 360
- Foellmi C., Moffat A. F. J., Guerrero M. A., 2003b, *MNRAS*, 338, 1025
- Fox D. W. et al., 2002a, GCNC 1564
- Fox D. W. et al., 2002b, GCNC 1569
- Fox D. W. et al., 2003, *Nat*, 422, L284
- Fynbo J. P. U. et al., 2004, *ApJ*, submitted
- Galama T. J. et al., 1998, *Nat*, 395, 670
- Garnavich P. M. et al., 2003, *ApJ*, 582, 924
- Gosachinskij I. V., Lozinskaya T. A., 2002, *AstL*, 28, 701
- Heyl J. S., Perna R., 2003, *ApJ*, 586, L17
- Hjorth J. et al., 2003, *Nat*, 423, 847
- Holland S. T. et al., 2002, *AJ*, 124, 639
- Holland S. T. et al., 2003, *AJ*, 125, 2291
- Howarth I. D., Phillips A. P., 1986, *MNRAS*, 222, 809

- Laursen L. T., Stanek K. Z., 2003, *ApJ*, 597, 107
- Lazzati D., Rossi E., Covino S., Ghisellini G., Malesani D., 2002, *A&A*, 396, L5
- Lee C.-H., Brown G. E., Wijers R. A. M. J., 2002, *ApJ*, 575, 996
- Leitherer C., Lamers H. J. G. L. M., 1991, *ApJ*, 373, 89
- Li Z.-Y., Chevalier R., 2003, *ApJ*, 589, L69
- Lipkin Y. M. et al., 2004, *ApJ*, 606, 381
- Malesani D. et al., 2004, *ApJ*, 609, L5
- Marchenko S. V. et al., 2004, *MNRAS*, 353, 153
- Matheson T. et al., 2003, *ApJ*, 582, L5
- Metzger M. R., Djorgovski S. G., Kulkarni S. R., Steidel C. C., Adelberger K. L., Frail D. A., Costa E., Frontera F., 1997, *Nat*, 387, 878
- Mirabal N. et al., 2003, *ApJ*, 595, 935
- Møller P. et al., 2002, *A&A*, 396, L21
- Nakar E., Piran T., Granot J., 2003, *New Astronomy*, 8, 495
- Nussbaumer H., Schmutz W., Smith L. J., Willis A. J., 1982, *A&AS*, 47, 257
- Pandey S. B. et al., 2003, *BASI*, 31, 19
- Puls J. et al., 1996, *A&A*, 305, 171
- Salamanca I., Rol E., Wijers R. A. M. J., Kaper L., Ellison S., Tanvir N., 2002, GCNC 1611
- Schaefer B. E. et al., 2003, *ApJ*, 588, 387
- Schlegel D. J., Finkbeiner D. P., Davis M., 1998, *ApJ*, 500, 525
- Shapley A. E., Steidel C. C., Pettini M., Adelberger K. L., 2003, *ApJ*, 588, 65
- Shirasaki Y. et al., 2002, GCNC 1565
- Stanek K. Z., Garnavich P. M., Kaluzny J., Pych W., Thompson I., 1999, *ApJ*, 522, L39
- Stanek K. Z. et al., 2003, *ApJ*, 591, L17
- Uemura M., Kato T., Ishioka R., Yamaoka H., 2003, *PASJ*, 55, L31
- Van Dokkum P. G., 2001, *PASP*, 113, 1420
- Van Marle A.-J., Langer N., García-Segura G., 2005, to appear in the proceedings of 'Gamma-ray Bursts in the Afterglow Era: 4th Workshop', Rome, Eds L. Piro, L. Amati, S. Covino and B. Gendre
- Verner D. A., Ferland G. J., Korista K. T., Yakovlev D. G., 1996, *ApJ*, 465, 487
- Vreeswijk P. M. et al., 2004, *A&A*, 419, 927
- Willis A. J., Crowther P. A., Fullerton A. W., Hutchings J. B., Sonneborn G., Brownsberger K., Massa D. L., Walborn N. R., 2004, *ApJS*, 154, 651

This paper has been typeset from a  $\text{\TeX}$ / $\text{\LaTeX}$  file prepared by the author.